Static and dynamic properties of noncollinear magnetized ferromagnetic films

J. Jiménez-Bustamante,[1] A. Lindner,[2] H. N. Koyun,[2] R. Salikhov,[2] K. Lenz,[2] J. Lindner,[2] and R. A. Gallardo[1,*]

[1]*Departamento de Física, Universidad Técnica Federico Santa María, Avenida España 1680, Valparaíso, Chile*

[2]*Helmholtz-Zentrum Dresden-Rossendorf, Institute of Ion Beam Physics and Materials Research, Bautzner Landstrasse 400, 01328 Dresden, Germany*

(Received 16 June 2023; accepted 7 February 2024; published 4 March 2024)

The dynamic matrix method was employed to perform theoretical calculations for investigating both static and dynamic characteristics of thick ferromagnetic films. This approach considers situations where a noncollinear equilibrium magnetization exists along the thickness due to a thickness-dependent uniaxial anisotropy and interfacial interactions in a synthetic antiferromagnet. In the former scenario, the study exposes a correlation between noncollinear static magnetization and a nonmonotonic dependence of ferromagnetic resonance frequency, where a frequency decrease is observed at low fields in the unsaturated regime. Regarding the synthetic antiferromagnet structure, the research demonstrates noncoherent magnetization rotation in the spin-flop regime, with twisted magnetization states influencing the critical and nucleation fields that define the spin-flop region. The results of the investigation were compared to the macrospin approach, where the magnetization is assumed to be uniform along the thickness. The study suggests that the contribution of noncollinear magnetic moments may mimic the role of the biquadratic interaction in the macrospin model, implying that such a biquadratic term may be overestimated in coupled ferromagnetic films with thicknesses exceeding the material's intrinsic exchange length. Finally, the model was compared with experimental data obtained from a Py/Ir/Py synthetic antiferromagnet, demonstrating that the theoretical consideration of a twisting equilibrium state of the magnetization precisely reproduces the observed dynamic and static properties of the nanostructure.

DOI: 10.1103/PhysRevB.109.094403

I. INTRODUCTION

The static and dynamic properties of nanostructured magnetic systems have been widely studied due to their fundamental physics and technological application perspectives [1–4]. These structures can be classified into categories based mainly on their shape, composition, and magnetic properties. According to the shape, the magnetic nanostructures can be classified into magnetic nanoparticles [5–7], magnetic nanowires and nanotubes [8–12], ultrathin magnetic films [13,14], magnetic quantum dots [15,16], magnonic crystals [17–22], and magnetic superlattices [23–25], among others. Due to the complexity of the magnetization distribution and geometry of the nanomagnets, their physical properties have been studied mainly using computational tools [26–29]. Nonetheless, analytical or semianalytical theories are feasible in cases where the geometry of the nanostructure has some symmetries. For instance, magnetic nanotubes, magnetic stripes, and multilayers can be analytically modeled [9,30–36]. Similarly, spin textures such as domain walls and magnetic skyrmions can also be comprehensively investigated using analytical methods [37–41], enabling a better understanding of the underlying physics governing these magnetic systems.

The physical properties of small nanomagnets have been theoretically addressed utilizing the macrospin model [42]. In this model, the magnetic moments of the structure are considered as a single macroscopic entity with a fixed magnitude and orientation, which is only affected by an effective field, which includes contributions from the external magnetic field, exchange interactions, dipole-dipole interactions, and anisotropies. Nevertheless, such a model has some limitations. For instance, it does not account for the impact of thermal fluctuations on the particle's magnetic moment, which can alter its magnetic characteristics [43]. Moreover, the model does not consider the effects of surface interactions, which can be significant in certain types of nanostructures [44,45]. As the thickness of the nanostructure increases, for instance, there is a notable difference in the magnetic behavior of the moments at the interfaces compared to that of the bulk region due to variations in exchange coupling. Additionally, the system tries to avoid the formation of surface magnetic charges. As a result, a change in the equilibrium magnetization across the thickness is anticipated, rendering the macrospin model invalid. The variation in the equilibrium magnetization can be even further enlarged when nonuniform magnetic properties across the thickness are taken into account [46,47] or when the magnetic nanostructure exhibits significant interfacial interactions, such as surface anisotropies, Dzyaloshinskii-Moriya coupling, or the interlayer exchange interaction that is commonly observed in magnetic multilayers [48,49].

In films exhibiting a magnetic gradient across their thickness, the internal moments experience varying local fields, resulting in a change in the resonance frequency [46,50]. Moreover, when an external field is applied along the hard

*rodolfo.gallardo@usm.cl

axis, a twisting of the equilibrium magnetization is anticipated, which would be more prominent in thick films. Even a minor deviation from the equilibrium magnetization could result in a nonuniform equilibrium state that alters the frequency of magnetization excitations. Therefore, such nonuniform conditions must be taken into account to characterize the magnetic system accurately. Surface effects are a particular case of the magnetization graduation, where the properties of the systems suddenly change at the interfaces. In magnetic multilayers, an interfacial bilinear exchange interaction has been considered where, depending on the thickness of the nonmagnetic spacer that separates the ferromagnetic (FM) layers, oscillations between antiferromagnetic and ferromagnetic states have been observed [51–54]. Despite the bilinear interlayer exchange interaction, a biquadratic exchange has been phenomenologically introduced to explain the hysteresis curves in Fe/Cr/Fe trilayers [55,56]. Such a biquadratic term leads to a perpendicular orientation between neighboring magnetizations, resulting in an energetically favorable alignment at angles other than 0 or 180 degrees relative to each other [57,58]. Biquadratic interlayer exchange can play an essential role in a variety of magnetic systems, such as multilayered magnetic materials and two-dimensional magnets [59]. Although the influence of interfacial exchange interactions on thick magnetic layers is small, the pinning conditions caused by these interactions at the interfaces can result in variations of the equilibrium magnetization across the single-layer thickness, as previously mentioned. Therefore, it is essential to consider the equilibrium magnetization that varies along the thickness to provide an accurate theoretical description of the multilayer system. This factor can have an impact on both static and dynamic characteristics.

This paper studies the static and dynamic properties of ferromagnetic films with noncollinear equilibrium magnetization across the thickness. The theory that is employed is based on the dynamic matrix method, which subdivides the film system into multiple sublayers to account for variations in the magnetization across the thickness. The study investigates the equilibrium magnetization states and the ferromagnetic resonance response in a film with a nonuniform anisotropy profile across the thickness and a synthetic antiferromagnet. In the latter system, the interfacial interlayer exchange interaction results in a noncollinear magnetization rotation at low fields, creating a twisted magnetization state that plays a role similar to the well-known biquadratic exchange interaction.

II. THEORY

The system under study is shown in Fig. 1. Here, a ferromagnetic film with a noncollinear in-plane magnetization along the film's normal is considered, where such a rotated magnetization state can be induced by gradients of some magnetic parameter or interfacial effects that break the symmetry along the film thickness. The dynamic matrix method (DMM) is used to consider the variation of the magnetization along the thickness, where the idea is to divide the film into different sublayers or slabs connected through dipolar and exchange interactions [46,60]. This theoretical treatment is analogous to the Hamiltonian-based approach used in Refs. [61,62]. Nevertheless, the results presented here are generalized to consider magnetic graduation, and by using a convergence test, a continuous film is perfectly reproduced.

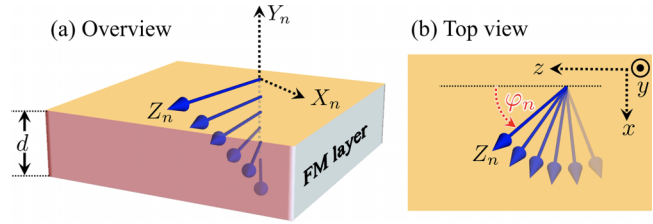

FIG. 1. Magnetic configuration of the ferromagnetic film, where the in-plane magnetization varies along the normal coordinate, as shown in the figure. (a) The reference frame (X_n, Y_n, Z_n) is a local coordinate system, where Z_n points along the equilibrium magnetization of the nth sublayer, X_n lies in the film's plane, and Y_n is normal to the plane. (b) The equilibrium magnetization makes an angle φ_n with respect to the z axis, which is associated with the reference frame (x, y, z). In this coordinate system, x is an easy axis and y is normal to the film's plane ($y = Y_n$).

The magnetization dynamic of the system is described by the Landau-Lifshitz (LL) equation of motion [63], which for the nth sublayer reads

$$\partial_t \mathbf{M}_n(\mathbf{r}, t) = -\gamma\mu_0 \mathbf{M}_n(\mathbf{r}, t) \times \mathbf{H}_n^{\mathrm{e}}(\mathbf{r}, t), \tag{1}$$

where $\mathbf{M}_n(\mathbf{r}, t)$ is the magnetization of sublayer n, γ is the magnitude of the gyromagnetic ratio, and $\mathbf{H}_n^{\mathrm{e}}(\mathbf{r}, t)$ is the effective field acting on sublayer n. Assuming small deviations of the magnetization around the equilibrium, both the magnetization and the effective field can be written as $\mathbf{M}_n(\mathbf{r}, t) = M_{\mathrm{s}_n}\hat{Z}_n + \mathbf{m}_n(\mathbf{r}, t)$ and $\mathbf{H}_n^{\mathrm{e}}(\mathbf{r}, t) = H_{Z_n}^{\mathrm{e}0}\hat{Z}_n + \mathbf{h}_n^{\mathrm{e}}(\mathbf{r}, t)$, respectively. Here, M_{s_n} is the saturation magnetization of the nth sublayer and $H_{Z_n}^{\mathrm{e}0}$ corresponds to the static Z_n component of the effective field. Vectors $\mathbf{m}_n(\mathbf{r}, t)$ and $\mathbf{h}_n^{\mathrm{e}}(\mathbf{r}, t)$ are the dynamic parts of the magnetization and effective field, respectively. By assuming a harmonic time dependence, dynamic magnetization can be written as $\mathbf{m}_n(\mathbf{r}, t) = \mathbf{m}_n(\mathbf{r})e^{i\omega t}$ (with $\omega = 2\pi f$). Thus, the LL equation becomes

$$i(\omega/\gamma\mu_0)m_{X_n}(y) = -m_{Y_n}(y)H_{Z_n}^{\mathrm{e}0} + M_{\mathrm{s}_n}h_{Y_n}^{\mathrm{e}}(y), \tag{2}$$

$$i(\omega/\gamma\mu_0)m_{Y_n}(y) = m_{X_n}(y)H_{Z_n}^{\mathrm{e}0} - M_{\mathrm{s}_n}h_{X_n}^{\mathrm{e}}(y). \tag{3}$$

In this study, the magnetization's spatial variation has only been considered along the normal coordinate y. This consideration is due to the equilibrium texture being examined (refer to Fig. 1) and the fact that modes with zero wave vector will be analyzed, such as ferromagnetic resonance modes, where there is no lateral variation of the magnetization. Equations (2) and (3) can be written as $i\omega\mathbf{m}_n(y) = \gamma\mu_0\tilde{\mathbf{A}}\mathbf{m}_n(y)$, where once the matrix elements are obtained (see the Appendix), the system can be solved as an eigenvalue problem.

Equations (2) and (3) also contain the equilibrium condition $H_{Y_n}^{\mathrm{e}0} = H_{X_n}^{\mathrm{e}0} = 0$. The case $H_{Y_n}^{\mathrm{e}0} = 0$ implicates that the equilibrium magnetization is in the plane. On the other side, the in-plane static component of the effective field $H_{X_n}^{\mathrm{e}0}$ contains the angle φ_n that needs to be found for every sublayer. Such a component is given by

$$H_{X_n}^{\mathrm{e}0} = H\sin(\varphi_H - \varphi_n) + \frac{H_{\mathrm{u}_n}}{2}\sin(2\varphi_n) + \sum_{\eta} H_{n,\eta}^{\mathrm{C}}, \tag{4}$$

where H is the magnitude of the external field, φ_H is the angle that H makes with the z axis, and H_{u_n} is the uniaxial anisotropy of sublayer n, with x being the easy axis. The connection between sublayers n and η is established by a coupling field, denoted as $H^{C}_{n,\eta}$. This coupling field arises from exchange interactions between the sublayers for a thick ferromagnetic film partitioned into numerous sublayers. Thus, $H^{C}_{n,\eta}$ is

$$H^{C}_{n,\eta} = -\frac{J_I}{d_n \mu_0 M_{s_n}} \sin(\varphi_n - \varphi_\eta)\left(\delta_\eta^{n+1} + \delta_\eta^{n-1}\right), \quad (5)$$

where δ_i^j is the Kronecker delta function ($\delta_i^j = 0$ for $i \neq j$ and $\delta_i^j = 1$ for $i = j$), J_I is the intralayer exchange constant, and d_n is the thickness of the nth sublayer, with $d = N d_n$ the total thickness and N the total number of sublayers. Because several divisions are required to reach the continuous variation of the magnetization along the thickness, the results are analyzed regarding a convergence criterium. Thereby, the number of divisions is truncated once the convergence of the result is reached. In addition, as the number of divisions is significant, it is possible to show that $J_I = 2A_{ex}/d_n$ [3,46], where A_{ex} is the exchange constant defined in the continuum model. It is worth mentioning that the equilibrium magnetization can be alternatively determined by solving a differential equation for the angle φ_n, as demonstrated in previous works [64,65]. However, such an approach is not suitable for systems characterized by a gradient in the magnetic properties. In such cases, the dynamic matrix method proves to be a more practical and appropriate choice.

The present investigation also focuses on a synthetic antiferromagnet consisting of two ferromagnetic layers with antiferromagnetically coupled magnetizations. Hence, bilinear and biquadratic interlayer exchange interactions are considered in addition to the intralayer exchange interaction. Thus, the coupling field for a synthetic antiferromagnet ($H^{CSA}_{n,\eta}$) is given by

$$\begin{aligned} H^{CSA}_{n,\eta} = &-\frac{J_{bl}}{d_n \mu_0 M_{s_n}} \sin(\varphi_n - \varphi_\eta)\left(\delta_n^\alpha \delta_\eta^{\alpha+1} + \delta_n^{\alpha+1}\delta_\eta^\alpha\right) \\ &-\frac{J_{bq}}{d_n \mu_0 M_{s_n}} \sin[2(\varphi_n - \varphi_\eta)]\left(\delta_n^\alpha \delta_\eta^{\alpha+1} + \delta_n^{\alpha+1}\delta_\eta^\alpha\right) \\ &+H^{C}_{n,\eta}\left(1 - \delta_n^\alpha \delta_\eta^{\alpha+1} - \delta_n^{\alpha+1}\delta_\eta^\alpha\right). \end{aligned} \quad (6)$$

Here, J_{bl} is the bilinear exchange constant, while J_{bq} is the biquadratic strength. Moreover, sublayers α and $\alpha + 1$ are located at the interface that separates the FM layers. Thus, the bilinear and biquadratic interactions only exist at such an interface. Note that in the last term of Eq. (6), the δ functions are included to delete the term $H^{C}_{n,\eta}$ when the coupling is given between sublayers α and $\alpha + 1$.

III. RESULTS AND DISCUSSION

In the following discussion, the parameters of the cobalt material are used as a reference. Namely, the saturation magnetization is $M_s = 1200$ kA/m and the exchange constant is $A_{ex} = 18$ pJ/m (exchange length $\ell_{ex} = 4.46$ nm). Regarding the application of the DMM, a total of $N = 40$ divisions is used to guarantee the convergence of the results. Two exemplary systems will be studied. The first corresponds to a single layer with nonhomogeneous uniaxial anisotropy, where different anisotropy profiles are considered. The second system is a typical synthetic antiferromagnet structure, where the antiparallel alignment of the magnetizations is promoted by an interlayer exchange interaction with $J_{bl} < 0$. Both systems are consistent with a noncollinear magnetization rotation when an external field is applied along the film plane. In Fig. 2, different anisotropy profiles are considered for an FM film with $d = 40$ nm. For comparison, the same average anisotropy has been considered in all cases ($\langle \mu_0 H_u \rangle = 100$ mT). The easy axis is given by x, while the external field is applied along z ($\varphi_H = 0$). Figures 2(a)–2(c) depict the case of a uniform anisotropy profile (case 1). Figure 2(b) shows a uniform (across the thickness) magnetization reorientation as an external field along the hard axis is increased. Figure 2(c) illustrates the two ferromagnetic low-frequency resonance modes within the frequency range of 0–30 GHz, with higher-order modes being excited at frequencies beyond this range, although they are not presented in the figure. The solid line represents the uniform in-phase mode, while the dashed line corresponds to the first excited out-of-phase mode. Here, it is observed that the frequency becomes zero at the nucleation field ($\mu_0 H_N$), defined as the field in which the first deviation from a uniformly magnetized state appears. Case 2 shows an example of a nonuniform anisotropy, as illustrated in Figs. 2(d)–2(f), where the anisotropy parameter has a gradual variation across the film thickness. The magnetization equilibrium angle is shown in Fig. 2(e), where a clear twisted state of the magnetization is observed before the saturation at $\mu_0 H_N \approx 122$ mT, as shown in Fig. 2(f)]. The magnetic moments with low-local anisotropy [darker points in Fig. 2(e)] follow the external field first and then follow the rest of the magnetization. The frequency-field dependence of the modes does not notably change [see Figs. 2(c) and 2(f)], but the nucleation field increases due to the zones with high anisotropy. Finally, an interfacial-like anisotropy profile is considered in case 3, where the effective anisotropy field is localized at the surface of the FM layer, as shown in Fig. 2(g). Here, the noncollinear magnetization state is enhanced due to the strong nonhomogeneity of the anisotropy, as shown in Fig. 2(h). The magnitude of the nucleation field significantly exceeds that of the previous cases, being more than three times larger than in the uniform scenario. As the thickness decreases, the difference between the nucleation fields for uniform and nonuniform anisotropies is reduced because the exchange interaction dominates, forcing the magnetic moments to rotate coherently. This behavior is evidenced in the inset of Fig. 2(g), where the nucleation field (calculated for an anisotropy profile of case 3) is shown as a function of the thickness. On the other side, the frequency of the low-frequency mode is reduced at small fields [see solid line in Fig. 2(i)], reaching a maximum at around $\mu_0 H =$ 200 mT. This dynamic behavior can be explained through the calculations of the magnetization profiles that are represented by the in-plane dynamic magnetization component m_{X_n}, as shown in the insets of Fig. 2(i). At small fields, the magnetization oscillates with a large amplitude on the zones with reduced anisotropy; therefore, it implies that the frequency of such modes is low due to the reduction of the local internal field. As the external field increases, the oscillation amplitude gradually increases in the high anisotropy region [lighter

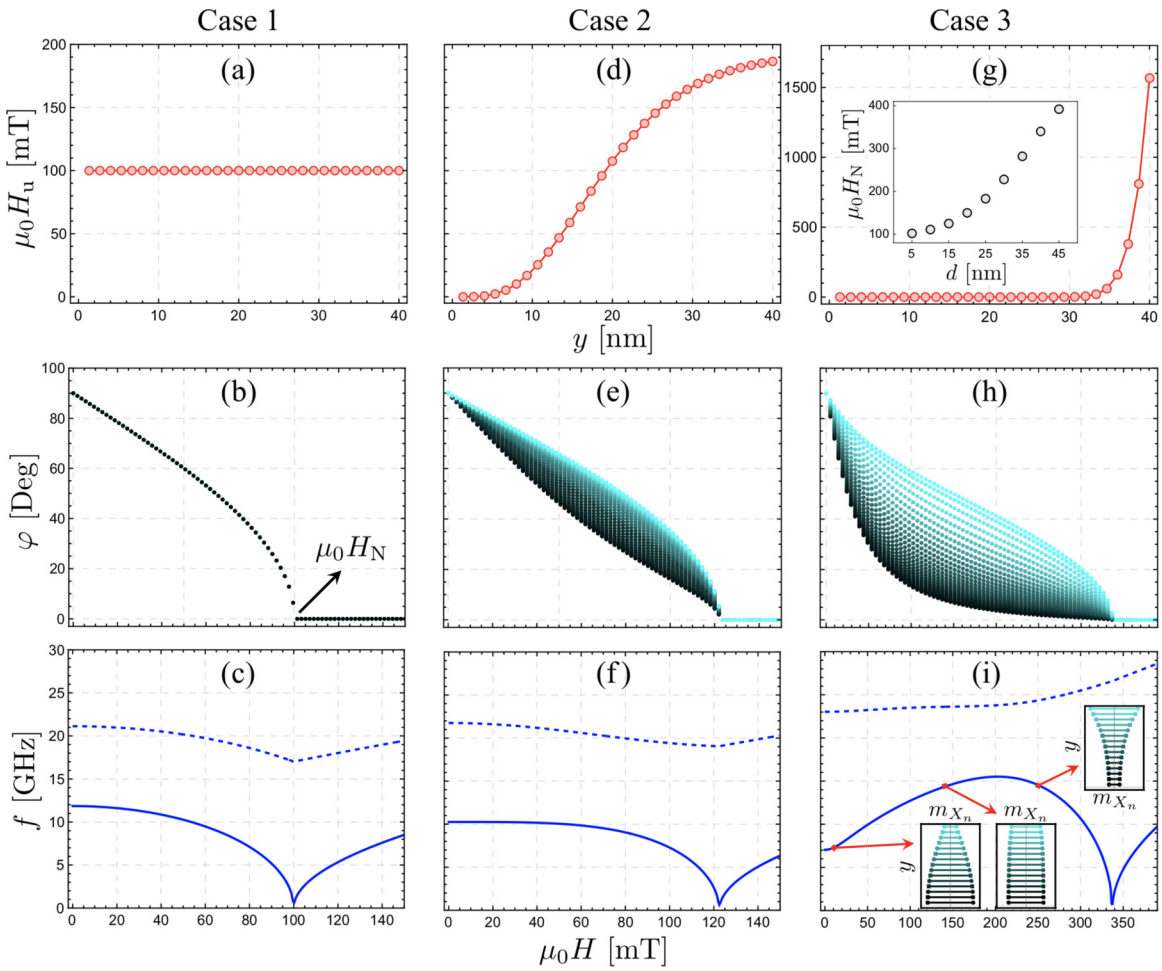

FIG. 2. Static and dynamic properties of a ferromagnetic film with a nonhomogeneous anisotropy profile evaluated for $d = 40$ nm. In (a)–(c), a constant anisotropy is considered, while in (d)–(f), a modulation in the whole bulk is assumed. An interfacial-like anisotropy profile is used in (g)–(i). The top panels show the anisotropy profile, the central panels depict the magnetization's in-plane equilibrium angle, and the lower panels show the ferromagnetic resonance frequency f as a function of the external field. The darker (lighter) points in (e) and (h) correspond to the magnetization located at the zones with low (high) anisotropy. The inset in (g) illustrates the nucleation field $\mu_0 H_N$ as a function of the film thickness. The insets in (i) correspond to the in-plane dynamic magnetization components evaluated at $\mu_0 H = 10$, 140, and 250 mT. In plots (c), (f), and (i), the solid line represents the in-phase uniform mode, while the dashed line corresponds to the first excited out-of-phase mode.

lines in the insets of Fig. 2(i)], thus increasing the frequency. However, as the external field increases further, the frequency reduces again because the amplitude of the oscillations becomes significant in the zones with high anisotropy, where, in turn, the magnetic moments are not fully oriented along the external field direction [66].

Now, the case of a synthetic antiferromagnet is addressed. Here, the interfacial nature of the interlayer exchange interaction is responsible for the noncoherent rotation of the magnetization under the application of an external field. Figure 3 shows three cases where the thicknesses of the individual layers have been varied for a symmetric antiferromagnet ($d_1 = d_2$), while an interlayer interaction strength (bilinear exchange term) of $J_{bl} = -1$ mJ/m^2 is used to remain the antiferromagnetic state stable at a zero applied field, $\mu_0 H = 0$. An in-plane uniaxial anisotropy of $\mu_0 H_u = 100$ mT is implemented to the bottom layer, resulting in the magnetization of this layer remaining parallel to the external field at small fields [see inset in Fig. 3(a)]. As expected, three distinctive regions are obtained by applying an external field along the easy axis ($\varphi_H = 90°$). In small fields, the magnetizations remain antiparallel. Then, at a critical field $\mu_0 H_c$, the antiferromagnetic state becomes unstable and the magnetizations begin to rotate. This intermediate state is called a spin-flop regime [67,68], which is an equilibrium configuration where the magnetizations are neither antiparallel nor parallel [see Fig. 3(e)]. As the external field increases further, the saturated state is reached at $\mu_0 H = \mu_0 H_N$, where $\mu_0 H_N$ is the nucleation field defined above. According to the model presented in this paper, the magnetic moments do not evolve coherently during the rotation in the spin-flop zone; instead, they describe a noncoherent rotation caused by the interfacial interlayer exchange interaction that couples the magnetization more strongly in the nonmagnetic/ferromagnetic interfaces. The magnetization angles at the bottom and top of the film ($y = 0$ and $y = 40$ nm, respectively) are closer to the external-field angle $\varphi_H = 90°$. This behavior is observed in the inset of Fig. 3(b) for the case $d_1 = d_2 = 20$ nm, where the equilibrium

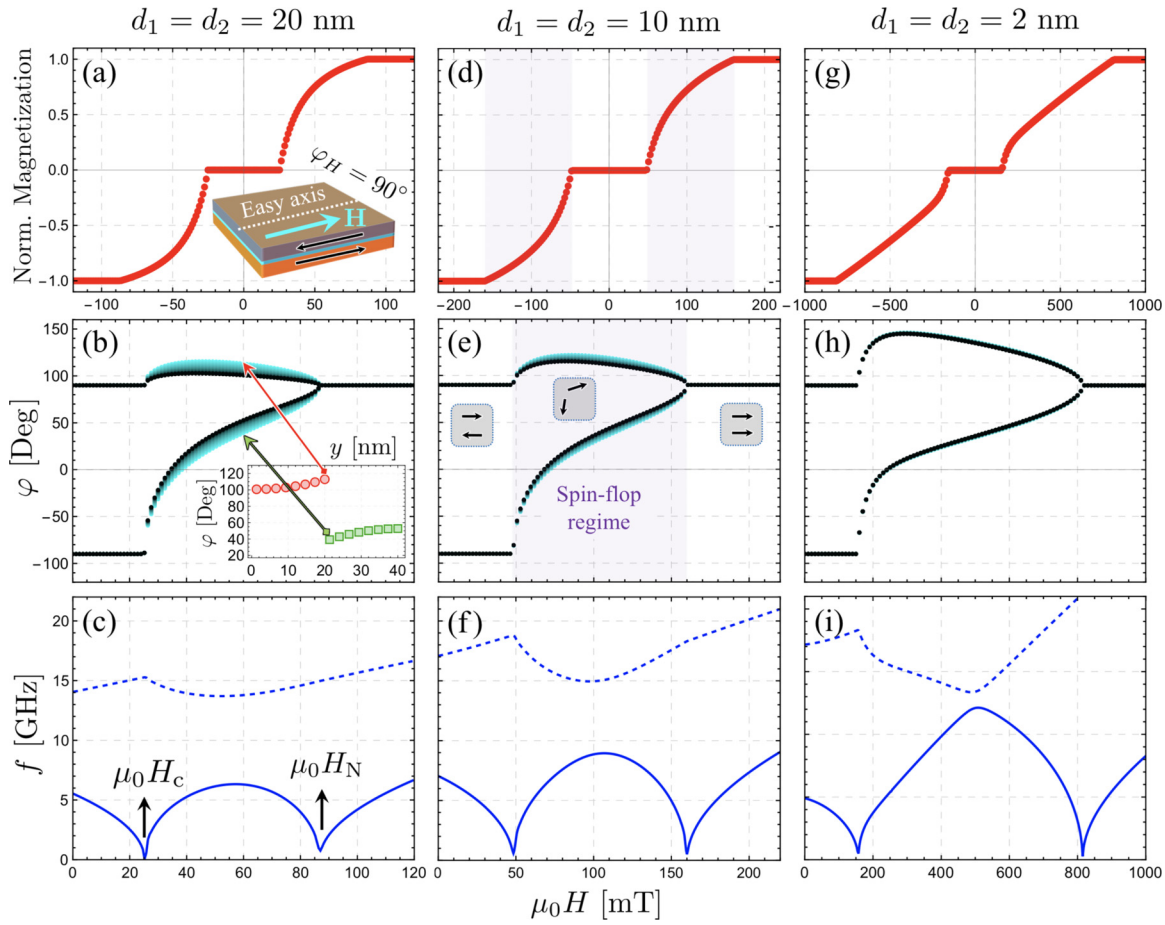

FIG. 3. Hysteresis loop, equilibrium angles, and ferromagnetic resonance frequency of synthetic antiferromagnetic nanostructures. In all cases, the external field is applied along the easy axis x ($\varphi_H = 90°$). (a)–(c), (d)–(f), and (g)–(i) correspond to the cases $d_1 = d_2 = 20$ nm, $d_1 = d_2 = 10$ nm, and $d_1 = d_2 = 2$ nm, respectively. In (b), (e), and (h), the lighter color in the curves represents the magnetic moments at the nonmagnetic/ferromagnetic interfaces, while the darker points correspond to the magnetization at the top/bottom of the films. The inset in (b) shows the twisting equilibrium angles of both layers as a function of the normal coordinate y evaluated at $\mu_0 H = 60$ mT. Circles correspond to the bottom layer, while squares represent the equilibrium angle of the top layer. The spin-flop regime is highlighted in (e). In plots (c), (f), and (i), the two low-frequency modes, also referred to as optic and acoustic modes, are illustrated as a function of the external field.

angles are evaluated at $\mu_0 H = 60$ mT. The equilibrium angles of the magnetic moments at the interfaces are described by the lighter curves in Fig. 3(b), while the darker points correspond to the magnetization angles at the top and bottom of the film. As the thicknesses of the ferromagnetic layers decrease, the magnetization rotation becomes more coherent, which is caused by the intralayer exchange energy, as mentioned above [see Figs. 3(e) and 3(h)]. In Figs. 3(c), 3(f), and 3(i), two low-frequency modes, known as the optic and acoustic modes, are depicted as a function of the external magnetic field. The assignment of optic and acoustic characteristics is based on the phase of magnetization oscillations, which undergoes a change within the spin-flop zone, as detailed in Ref. [68].

Now, the model based on the dynamic matrix method (DMM) is compared with the macrospin (MCS) model, which assumes that the magnetization is uniform in the whole thickness of the magnetic material. The case $d_1 = d_2 = 20$ nm is taken as an example to analyze both models in Fig. 4. The first quadrant of the hysteresis loop at positive fields is shown in Fig. 4(a), where the DMM model that considers noncoherent magnetization (solid orange circles) is compared with the macrospin approach (blue dashed lines). As observed, both models do not match perfectly, which is seen by the mismatch between the fields $\mu_0 H_c$ and $\mu_0 H_N$. Nevertheless, including the well-known biquadratic exchange term, described by the constant J_{bq}, into the MCS model (see the Appendix), it is possible to reach the results based on the noncoherent approach described in this paper. The comparison between MCS + J_{bq} (solid black line) and DMM is depicted in Fig. 4(a), where the inset of this figure shows that the dynamic response (frequency vs external field) also matches under the inclusion of J_{bq}. Of course, the requirement of a good agreement between the different models implicates that in the MCS + J_{bq} approach, the bilinear exchange constant J_{bl} must be modified, while in the DMM, it is fixed to be $J_{bl} = -1$ mJ/m^2. Figure 4(b) shows the critical and nucleation fields ($\mu_0 H_c$ and $\mu_0 H_N$, respectively) as a function of the layer thickness d_i, where $d_i = d_1 = d_2$. Here, the discrepancies between the MCS and DMM models are observed for the different thicknesses, while the case MCS + J_{bq} matches perfectly under a modification of the interlayer exchange constant and the inclusion of J_{bq}, as shown in the

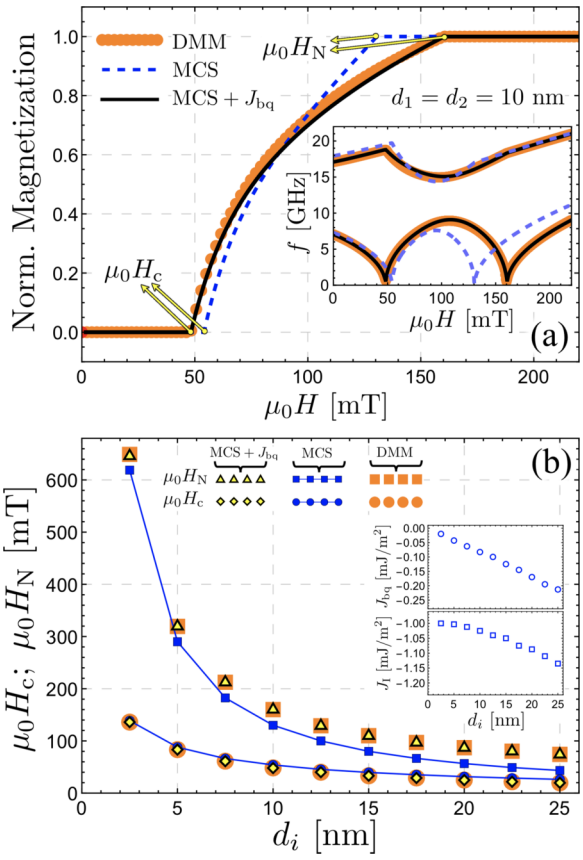

FIG. 4. (a) The first quadrant of the hysteresis loop for the case $d_1 = d_2 = 10$ nm. Orange markers show the dynamic matrix method (DMM) results, while the dashed (solid) line corresponds to the macrospin (macrospin plus J_{bq}) model. The inset in (a) depicts the ferromagnetic resonance frequency as a function of the external field. (b) Critical and nucleation fields as a function of the external field, where the DMM, MCS, and MCS + J_{bq} models are compared. The matching between DMM and MCS + J_{bq} is reached by modifying the interlayer exchange constant J_{bl} and including J_{bq}, as shown in the inset in (b). For the DMM case, the interlayer exchange constant is fixed as $J_{bl} = -1$ mJ/m^2.

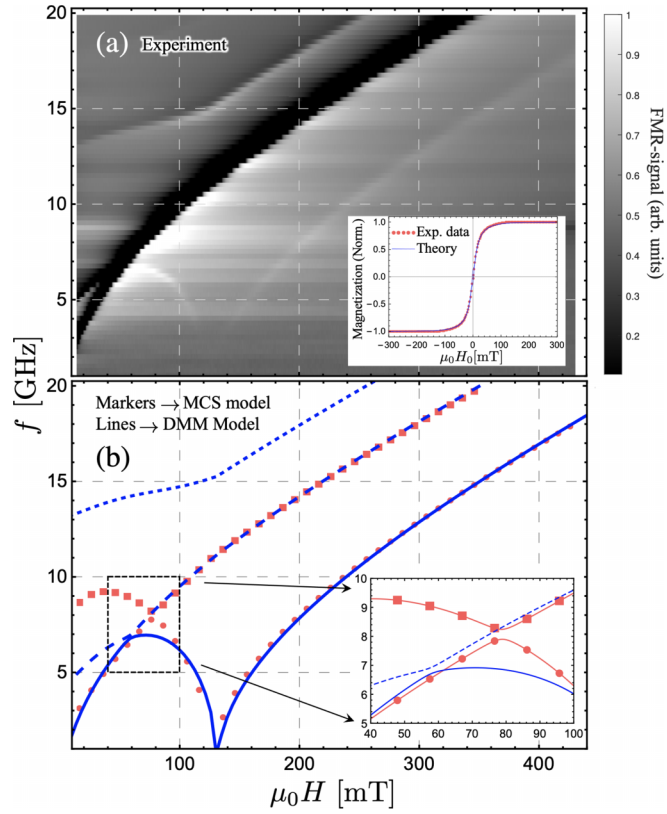

FIG. 5. (a) Frequency as a function of the external field. Color code represents the ferromagnetic resonance (FMR) signal in arbitrary units. The hysteresis loop is shown in the inset, where dots represent the measurements, and the lines are obtained from the DMM model. (b) Markers (dots and squares) and lines correspond to the calculated results using the MCS and DMM models, respectively. The inset in (b) illustrates the frequency range close to the avoided-crossing gap, which appears due to the thickness asymmetry of the stack. The parameters that are utilized for the calculations are described in the text.

inset of Fig. 4(b). An essential remark regarding these results is that the effects induced by the noncoherent rotation of the magnetization can be captured into the MCS model by including a biquadratic interaction. This implies that the contribution of the biquadratic term, typically associated with interface morphology characteristics, might be overestimated in the case of thick ferromagnetic films, where magnetization twisted states are feasible. In the context of thin or ultrathin film bilayers, the emergence of distinctive twisted states within the equilibrium magnetization is precluded by the intralayer exchange coupling. Consequently, the macrospin model effectively captures both the static and dynamic properties of these synthetic antiferromagnets [55,56,69–73]. In addition, a rotated state is also dependent on the strength of the interlayer exchange constant J_{bl}—a parameter intricately linked to spacer thickness. Namely, if J_{bl} is small, the rotated states are absent even for thick films, making the macrospin model again appropriate for describing the system's behavior.

Finally, a comparison is realized between the theoretical approach and the static and dynamic measurements conducted on a synthetic antiferromagnet consisting of two ferromagnetic layers made of permalloy (Py) separated by an iridium (Ir) spacer. The thicknesses of the Py films are 40 and 30 nm, while the Ir thickness is 0.4 nm [Py(40)/Ir(0.4)/Py(30)], respectively. Due to the nature of the Ir spacer, an antiferromagnetic state is induced between the FM layers ($J_{bl} < 0$) [74]. The gray color code in Fig. 5(a) illustrates the experimental results for the frequency as a function of the external field, $f(H)$, while the inset depicts the hysteresis loop. Both measurements [$f(H)$ and the hysteresis loop] are compared with the model presented in this paper [lines in Fig. 5(b)], where one can observe that the model reproduces the data perfectly using the following parameters: $M_s^{Py} = 791$ kA/m, $A_{ex}^{Py} = 9$ pJ/m, $J_{bl} = -0.6$ mJ/m^2, and $J_{bq} = -0.06$ mJ/m^2. In contrast, the macrospin model (MCS) is not able to reproduce the data quantitatively in the range of small fields ($H < H_N$). Indeed, the frequency of the high-frequency mode is inconsistent with the experiments (see squares at $\mu_0 H < 80$ mT). Only a qualitative agreement is

reached in this case, where the fitted parameters are $J_{\rm bl} = -0.7$ mJ/m^2 and $J_{\rm bq} = -0.5$ mJ/m^2 ($M_{\rm s}^{\rm Py}$ and $A_{\rm ex}^{\rm Py}$ are the same as previously used). The inset in Fig. 5(a) illustrates the frequency gap resulting from avoided crossing, an effect attributed to the thickness asymmetry of the synthetic antiferromagnet [72,73,75]. While both models exhibit this mode coupling, the observation occurs at distinct frequency and wave-vector ranges for each. Comparing the two theoretical models makes it apparent that the MCS model necessitates a substantial value of the biquadratic exchange to replicate the data qualitatively. Indeed, the MCS approach employs a value of $J_{\rm bq}$ that is approximately nine times greater than that used in the DMM. Therefore, the correct calculations of the rotated ground state significantly change the magnitude of the biquadratic exchange constant. This observation carries significant implications, suggesting that the biquadratic term could have been inaccurately treated and derived in prior studies of thick films where the equilibrium magnetization configuration displays a degree of torsion along the thickness. Incorporating the rotated magnetization configuration into the model substantially reduces the biquadratic interaction's strength, aligning with its interfacial nature. A considerable magnitude of the biquadratic exchange constant is found in the literature when the coupled layers have a thickness exceeding the material's intrinsic exchange length ($\ell_{\rm ex} = \sqrt{2A_{\rm ex}/\mu_0 M_{\rm s}^2}$) [76–81], where the macrospin model has been used to reproduce the measurements. In Ref. [78], for instance, the $f(H)$ curve is similar to the one illustrated in Fig. 5 for a sample [Py(30)/Ru(0.49)/Py(30)] (see Fig. 1(a) of Ref. [78]), where the MCS model requires a biquadratic constant of $J_{\rm bq} = -0.514$ mJ/m^2.

A further noteworthy observation depicted in Fig. 5 is that both models (MCS and DMM) exhibit exceptional agreement with the measurements in the saturated region ($\mu_0 H > \mu_0 H_{\rm N} \approx 122$ mT), despite employing highly distinct parameters for the interfacial exchange interactions. Hence, based on the findings of this study, for accurate magnetic characterization of the nanostructure, it is necessary to examine the regions preceding ($\mu_0 H < \mu_0 H_{\rm N}$) and succeeding ($\mu_0 H > \mu_0 H_{\rm N}$) the point of saturation. This analysis may not be crucial in thin films with minimal magnetic texture throughout their thickness. However, the analysis of the rotated states is fundamental for thick ferromagnetic films that exhibit interfacial or even graded magnetic properties.

IV. CONCLUSIONS

The study investigated the static and dynamic properties of noncollinear magnetization states in two nanostructures: a ferromagnetic film with nonuniform anisotropy along its thickness and a synthetic antiferromagnet. In both cases, it is found that the equilibrium magnetization develops a twisted state along the thickness under the application of an external field. This twisted configuration affects the resonance frequency of the system and the nucleation field. In the case of the synthetic antiferromagnet composed of thick ferromagnetic films, a rotated equilibrium magnetization state is observed that mimics the role of the biquadratic interaction. The findings suggest that the biquadratic exchange interaction in thick coupled films can be easily overestimated if the magnetization texture formed along the thickness is not considered. These results have significant implications from both a fundamental and practical perspective and provide a better understanding of the static and dynamic properties of thick ferromagnetic films.

ACKNOWLEDGMENTS

Support from FONDECYT, Grant No. 1210607, is highly acknowledged. J.J.-B. acknowledges the support of PIIC Grant No. 032/2022. The authors thank T. Naumann (HZDR) for technical support and thin-film deposition.

APPENDIX: MATRIX ELEMENTS

The components of $\tilde{\mathbf{A}}$ are determined by the energetic interactions present in the magnetic nanostructure. The energetic terms include Zeeman, demagnetizing, in-plane uniaxial anisotropy, and interlayer exchange terms. In this work, the interlayer terms arise only in the case of a synthetic antiferromagnet, where the bilinear and biquadratic exchange interactions are accounted for. The energy density associated with the bilinear and biquadratic terms is expressed as

$$\epsilon_{ij} = -J_{\rm bl}\frac{\mathbf{M}_i \cdot \mathbf{M}_j}{M_{{\rm s}_i} M_{{\rm s}_j}} - J_{\rm bq}\left(\frac{\mathbf{M}_i \cdot \mathbf{M}_j}{M_{{\rm s}_i} M_{{\rm s}_j}}\right)^2.$$

Here, i and j represent the sublayers at the interface of the two FM films (denoted as α and $\alpha + 1$). When $J_{\rm bl}$ is the dominant term and its value is negative, the magnetization of the films will be antiparallel at zero external field. Conversely, if $J_{\rm bq}$ is the dominant term and also negative, the magnetizations of the layers will tend to be perpendicular to each other. The effective interlayer exchange fields acting on the ith layer can be obtained from $\mathbf{H}_i^{\rm ex} = -(\mu_0 d_i)^{-1}\partial_{\mathbf{M}_i}\epsilon_{ij}$. In the same way, the effective fields associated with the Zeeman, demagnetizing, and uniaxial anisotropy can be obtained (see details in Ref. [34]).

By considering the dynamic effective field components as

$$h_{\xi_n}^{\rm e}(\mathbf{r}) = \sum_{\xi'}\sum_{\eta}\Gamma_{\xi_n,\xi'_\eta} m_{\xi'_\eta},$$

with $\xi_n = X_n, Y_n$, the matrix elements of $\tilde{\mathbf{A}}$ can be derived as follows:

$$\mathrm{A}_{Y_n Y_\eta} = \begin{cases} M_{{\rm s}_n}\Gamma_{X_n,Y_\eta}, & n \neq \eta \\ M_{{\rm s}_n}\Gamma_{X_n,Y_n}, & n = \eta, \end{cases}$$

$$\mathrm{A}_{X_n X_\eta} = \begin{cases} -M_{{\rm s}_n}\Gamma_{Y_n,X_\eta}, & n \neq \eta \\ -M_{{\rm s}_n}\Gamma_{Y_n,X_n}, & n = \eta, \end{cases}$$

$$\mathrm{A}_{Y_n X_\eta} = \begin{cases} M_{{\rm s}_n}\Gamma_{X_n,X_\eta}, & n \neq \eta \\ M_{{\rm s}_n}\Gamma_{X_n,X_n} - H_{Z_n}^{\rm e0}, & n = \eta, \end{cases}$$

and

$$\mathrm{A}_{X_n Y_\eta} = \begin{cases} -M_{{\rm s}_n}\Gamma_{Y_n,Y_\eta}, & n \neq \eta \\ -M_{{\rm s}_n}\Gamma_{Y_n,Y_n} + H_{Z_n}^{\rm e0}, & n = \eta. \end{cases}$$

The Γ_{ξ_n,ξ'_η} terms are $\Gamma_{X_n,Y_n} = \Gamma_{Y_n,X_n} = \Gamma_{X_n,Y_\eta} = \Gamma_{Y_n,X_\eta} = 0$, $\Gamma_{Y_n,Y_n} = -1$, and

$$\Gamma_{X_n,X_n} = \sum_\eta \frac{2J_{\mathrm{bq}}}{d_n\mu_0 M_{\mathrm{s}_n}} \sin^2(\varphi_n - \varphi_\eta)\left(\delta_n^\alpha \delta_\eta^{\alpha+1} + \delta_n^{\alpha+1}\delta_\eta^\alpha\right) + \frac{H_{\mathrm{u}_n}}{M_{\mathrm{s}_n}} \cos(\varphi_n)^2,$$

$$\Gamma_{X_n,X_\eta} = \frac{J_{\mathrm{I}} \cos(\varphi_n - \varphi_\eta)}{d_n\mu_0 M_{\mathrm{s}_n} M_{\mathrm{s}_\eta}}\left(\delta_\eta^{n+1} + \delta_\eta^{n-1}\right) + \frac{J_{\mathrm{bl}} \cos(\varphi_n - \varphi_\eta)}{d_n\mu_0 M_{\mathrm{s}_n} M_{\mathrm{s}_\eta}}\left(\delta_n^\alpha \delta_\eta^{\alpha+1} + \delta_n^{\alpha+1}\delta_\eta^\alpha\right) + \frac{J_{\mathrm{bq}} \cos[2(\varphi_n - \varphi_\eta)]}{d_n\mu_0 M_{\mathrm{s}_n} M_{\mathrm{s}_\eta}}\left(\delta_n^\alpha \delta_\eta^{\alpha+1} + \delta_n^{\alpha+1}\delta_\eta^\alpha\right),$$

and

$$\Gamma_{Y_n,Y_\eta} = \frac{J_{\mathrm{I}}}{d_n\mu_0 M_{\mathrm{s}_n} M_{\mathrm{s}_\eta}}\left(\delta_\eta^{n+1} + \delta_\eta^{n-1}\right) + \frac{J_{\mathrm{bl}}}{d_n\mu_0 M_{\mathrm{s}_n} M_{\mathrm{s}_\eta}}\left(\delta_n^\alpha \delta_\eta^{\alpha+1} + \delta_n^{\alpha+1}\delta_\eta^\alpha\right) + \frac{2J_{\mathrm{bq}} \cos(\varphi_n - \varphi_\eta)}{d_n\mu_0 M_{\mathrm{s}_n} M_{\mathrm{s}_\eta}}\left(\delta_n^\alpha \delta_\eta^{\alpha+1} + \delta_n^{\alpha+1}\delta_\eta^\alpha\right).$$

In the previous equations, H_{u_n} is the uniaxial anisotropy field, where the easy axis corresponds to x. In addition, it should be noted that J_{I} is null at the layers α and $\alpha + 1$, where the interlayer terms (bilinear and biquadratic) are present. Note that $A_{X_nY_n} = M_{\mathrm{s}_n} + H^{\mathrm{e0}}_{Z_n}$, where M_{s_n} accounts for the contribution of the demagnetizing field resulting from surface charges at the top and bottom of the sublayers, while the term $H^{\mathrm{e0}}_{Z_n}$ corresponds to the Z_n component of the effective static field and is defined as follows:

$$H^{\mathrm{e0}}_{Z_n} = H\cos(\varphi_H - \varphi_n) + H_{\mathrm{u}_n}\sin^2\varphi_n + \sum_\eta \frac{J_{\mathrm{I}}\cos(\varphi_n - \varphi_\eta)}{d_n\mu_0 M_{\mathrm{s}_n}}\left(\delta_\eta^{n+1} + \delta_\eta^{n-1}\right) + \sum_\eta \frac{J_{\mathrm{bl}}\cos(\varphi_n - \varphi_\eta)}{d_n\mu_0 M_{\mathrm{s}_n}}\left(\delta_n^\alpha \delta_\eta^{\alpha+1} + \delta_n^{\alpha+1}\delta_\eta^\alpha\right) + \sum_\eta \frac{2J_{\mathrm{bq}}\cos^2(\varphi_n - \varphi_\eta)}{d_n\mu_0 M_{\mathrm{s}_n}}\left(\delta_n^\alpha \delta_\eta^{\alpha+1} + \delta_n^{\alpha+1}\delta_\eta^\alpha\right).$$

It is important to note that the interactions between sublayers are exclusively of an exchange nature. When examining the system from a static point of view, and assuming a homogenous magnetization in the x and z directions, the dipolar interaction between sublayers becomes negligible due to the in-plane configuration of the twisted equilibrium magnetization. This implies that $\mathbf{M}_i \cdot \hat{n} = 0$ and $\nabla \cdot \mathbf{M}_i = \partial_y M_y = 0$ (since $M_y = 0$) for the surface and volumetric charges, respectively. Here, $\hat{n}$ represents the normal direction and M_y corresponds to the static normal component of the equilibrium magnetization. From a dynamic perspective, similar considerations apply. Within each ferromagnetic sublayer, magnetization is uniform, primarily because the FMR mode with a zero wave vector is analyzed. Consequently, there are no volumetric charges capable of inducing dipolar interactions between sublayers. In terms of dynamic surface charges, the uniformity of magnetization within each sublayer results in identical magnetic surface charges at both the top and bottom of the sublayer. As a result, beyond the sublayer boundaries, there are no dynamic stray fields induced by these surface magnetic charges, yielding a zero field.

[1] M. N. Baibich, J. M. Broto, A. Fert, F. Nguyen Van Dau, F. Petroff, P. Etienne, G. Creuzet, A. Friederich, and J. Chazelas, Giant magnetoresistance of (001)Fe/(001)Cr magnetic superlattices, Phys. Rev. Lett. **61**, 2472 (1988).

[2] M. T. Johnson, P. J. H. Bloemen, F. J. A. den Broeder, and J. J. de Vries, Magnetic anisotropy in metallic multilayers, Rep. Prog. Phys. **59**, 1409 (1996).

[3] V. Sluka, T. Schneider, R. A. Gallardo, A. Kákay, M. Weigand, T. Warnatz, R. Mattheis, A. Roldán-Molina, P. Landeros, V. Tiberkevich, A. Slavin, G. Schütz, A. Erbe, A. Deac, J. Lindner, J. Raabe, J. Fassbender, and S. Wintz, Emission and propagation of 1D and 2D spin waves with nanoscale wavelengths in anisotropic spin textures, Nat. Nanotechnol. **14**, 328 (2019).

[4] A. Barman, G. Gubbiotti, S. Ladak, A. O. Adeyeye, M. Krawczyk, J. Gräfe, C. Adelmann, S. Cotofana, A. Naeemi, V. I. Vasyuchka, B. Hillebrands, S. A. Nikitov, H. Yu, D. Grundler, A. V. Sadovnikov, A. A. Grachev, S. E. Sheshukova, J.-Y. Duquesne, M. Marangolo, G. Csaba *et al.*, The 2021 magnonics roadmap, J. Phys.: Condens. Matter **33**, 413001 (2021).

[5] R. H. Kodama, Magnetic nanoparticles, J. Magn. Magn. Mater. **200**, 359 (1999).

[6] S. P. Gubin, Y. A. Koksharov, G. B. Khomutov, and G. Y. Yurkov, Magnetic nanoparticles: preparation, structure and properties, Russ. Chem. Rev. **74**, 489 (2005).

[7] A.-H. Lu, E. L. Salabas, and F. Schüth, Magnetic nanoparticles: Synthesis, protection, functionalization, and application, Angew. Chem. Intl. Ed. **46**, 1222 (2007).

[8] L. Sun, Y. Hao, C.-L. Chien, and P. C. Searson, Tuning the properties of magnetic nanowires, IBM J. Res. Dev. **49**, 79 (2005).

[9] P. Landeros, S. Allende, J. Escrig, E. Salcedo, D. Altbir, and E. E. Vogel, Reversal modes in magnetic nanotubes, Appl. Phys. Lett. **90**, 102501 (2007).

[10] D. Lee, R. E. Cohen, and M. F. Rubner, Heterostructured magnetic nanotubes, Langmuir **23**, 123 (2007).

[11] J. Alam, C. Bran, H. Chiriac, N. Lupu, T. A. Óvári, L. V. Panina, V. Rodionova, R. Varga, M. Vazquez, and A. Zhukov, Cylindrical micro and nanowires: Fabrication, properties and applications, J. Magn. Magn. Mater. **513**, 167074 (2020).

[12] L. Piraux, Magnetic nanowires, Appl. Sci. **10**, 1832 (2020).

[13] B. Heinrich and J. F. Cochran, Ultrathin metallic magnetic films: magnetic anisotropies and exchange interactions, Adv. Phys. **42**, 523 (1993).

[14] D. L. Mills and S. M. Rezende, Spin damping in ultrathin magnetic films, in *Spin Dynamics in Confined Magnetic Structures II*, edited by B. Hillebrands and K. Ounadjela (Springer, Berlin, 2003), pp. 27–59.

[15] S. J. Lee, S. Souma, G. Ihm, and K. J. Chang, Magnetic quantum dots and magnetic edge states, Phys. Rep. **394**, 1 (2004).

[16] C. A. Downing and M. E. Portnoi, Magnetic quantum dots and rings in two dimensions, Phys. Rev. B **94**, 045430 (2016).

[17] M. Krawczyk and H. Puszkarski, Plane-wave theory of three-dimensional magnonic crystals, Phys. Rev. B **77**, 054437 (2008).

[18] G. Gubbiotti, S. Tacchi, M. Madami, G. Carlotti, A. O. Adeyeye, and M. Kostylev, Brillouin light scattering studies of planar metallic magnonic crystals, J. Phys. D: Appl. Phys. **43**, 264003 (2010).

[19] S. Tacchi, G. Duerr, J. W. Kłos, M. Madami, S. Neusser, G. Gubbiotti, G. Carlotti, M. Krawczyk, and D. Grundler, Forbidden band gaps in the spin-wave spectrum of a two-dimensional bicomponent magnonic crystal, Phys. Rev. Lett. **109**, 137202 (2012).

[20] A. V. Chumak, V. I. Vasyuchka, A. A. Serga, M. P. Kostylev, V. S. Tiberkevich, and B. Hillebrands, Storage-recovery phenomenon in magnonic crystal, Phys. Rev. Lett. **108**, 257207 (2012).

[21] M. Langer, F. Röder, R. A. Gallardo, T. Schneider, S. Stienen, C. Gatel, R. Hübner, L. Bischoff, K. Lenz, J. Lindner, P. Landeros, and J. Fassbender, Role of internal demagnetizing field for the dynamics of a surface-modulated magnonic crystal, Phys. Rev. B **95**, 184405 (2017).

[22] P. Alvarado-Seguel and R. A. Gallardo, Band structure of a one-dimensional bilayer magnonic crystal, Phys. Rev. B **100**, 144415 (2019).

[23] I. K. Schuller, S. Kim, and C. Leighton, Magnetic superlattices and multilayers, J. Magn. Magn. Mater. **200**, 571 (1999).

[24] V. V. Kruglyak, M. L. Sokolovskii, V. S. Tkachenko, and A. N. Kuchko, Spin-wave spectrum of a magnonic crystal with an isolated defect, J. Appl. Phys. **99**, 08C906 (2006).

[25] R. A. Gallardo, T. Schneider, A. Roldán-Molina, M. Langer, A. S. Núñez, K. Lenz, J. Lindner, and P. Landeros, Symmetry and localization properties of defect modes in magnonic superlattices, Phys. Rev. B **97**, 174404 (2018).

[26] M. Dvornik, Y. Au, and V. V. Kruglyak, Micromagnetic simulations in magnonics, in *Magnonics: from Fundamentals to Applications*, edited by S. O. Demokritov and A. N. Slavin (Springer, Berlin, 2013), pp. 101–115.

[27] A. Vansteenkiste, J. Leliaert, M. Dvornik, M. Helsen, F. Garcia-Sanchez, and B. V. Waeyenberge, The design and verification of MuMax3, AIP Adv. **4**, 107133 (2014).

[28] J. Leliaert and J. Mulkers, Tomorrow's micromagnetic simulations, J. Appl. Phys. **125**, 180901 (2019).

[29] C. Donnelly, A. Hierro-Rodríguez, C. Abert, K. Witte, L. Skoric, D. Sanz-Hernández, S. Finizio, F. Meng, S. McVitie, J. Raabe *et al.*, Complex free-space magnetic field textures induced by three-dimensional magnetic nanostructures, Nat. Nanotechnol. **17**, 136 (2022).

[30] T. Valet and A. Fert, Theory of the perpendicular magnetoresistance in magnetic multilayers, Phys. Rev. B **48**, 7099 (1993).

[31] K. Y. Guslienko, S. O. Demokritov, B. Hillebrands, and A. N. Slavin, Effective dipolar boundary conditions for dynamic magnetization in thin magnetic stripes, Phys. Rev. B **66**, 132402 (2002).

[32] K. Y. Guslienko, R. W. Chantrell, and A. N. Slavin, Dipolar localization of quantized spin-wave modes in thin rectangular magnetic elements, Phys. Rev. B **68**, 024422 (2003).

[33] A. L. González, P. Landeros, and Á. S. Núñez, Spin wave spectrum of magnetic nanotubes, J. Magn. Magn. Mater. **322**, 530 (2010).

[34] R. A. Gallardo, T. Schneider, A. K. Chaurasiya, A. Oelschlägel, S. S. P. K. Arekapudi, A. Roldán-Molina, R. Hübner, K. Lenz, A. Barman, J. Fassbender, J. Lindner, O. Hellwig, and P. Landeros, Reconfigurable spin-wave nonreciprocity induced by dipolar interaction in a coupled ferromagnetic bilayer, Phys. Rev. Appl. **12**, 034012 (2019).

[35] A. F. Franco, Intensity enhancement of ferromagnetic resonance modes in exchange coupled magnetic multilayers, New J. Phys. **22**, 013017 (2020).

[36] R. A. Gallardo, P. Alvarado-Seguel, and P. Landeros, High spin-wave asymmetry and emergence of radial standing modes in thick ferromagnetic nanotubes, Phys. Rev. B **105**, 104435 (2022).

[37] F. H. D. Leeuw, R. V. D. Doel, and U. Enz, Dynamic properties of magnetic domain walls and magnetic bubbles, Rep. Prog. Phys. **43**, 689 (1980).

[38] P. Landeros and A. S. Núñez, Domain wall motion on magnetic nanotubes, J. Appl. Phys. **108**, 033917 (2010).

[39] G. Finocchio, F. Büttner, R. Tomasello, M. Carpentieri, and M. Kläui, Magnetic skyrmions: from fundamental to applications, J. Phys. D: Appl. Phys. **49**, 423001 (2016).

[40] G. Yin, Y. Li, L. Kong, R. K. Lake, C. L. Chien, and J. Zang, Topological charge analysis of ultrafast single skyrmion creation, Phys. Rev. B **93**, 174403 (2016).

[41] R. Cheng, M. Li, A. Sapkota, A. Rai, A. Pokhrel, T. Mewes, C. Mewes, D. Xiao, M. De Graef, and V. Sokalski, Magnetic domain wall skyrmions, Phys. Rev. B **99**, 184412 (2019).

[42] A. Aharoni, *Introduction to the Theory of Ferromagnetism* (Oxford University Press, Oxford, 2000).

[43] W. F. Brown, Jr., Thermal fluctuations of a single-domain particle, Phys. Rev. **130**, 1677 (1963).

[44] D. Fiorani, *Surface Effects in Magnetic Nanoparticles* (Springer Science & Business Media, New York, 2005).

[45] J. Mazo-Zuluaga, J. Restrepo, and J. Mejía-López, Effect of surface anisotropy on the magnetic properties of magnetite nanoparticles: A Heisenberg–Monte Carlo study, J. Appl. Phys. **103**, 113906 (2008).

[46] R. A. Gallardo, P. Alvarado-Seguel, T. Schneider, C. Gonzalez-Fuentes, A. Roldán-Molina, K. Lenz, J. Lindner, and P. Landeros, Spin-wave non-reciprocity in magnetization-graded ferromagnetic films, New J. Phys. **21**, 033026 (2019).

[47] R. A. Gallardo, P. Alvarado-Seguel, A. Kákay, J. Lindner, and P. Landeros, Spin-wave focusing induced by dipole-dipole interaction in synthetic antiferromagnets, Phys. Rev. B **104**, 174417 (2021).

[48] P. Bruno, Theory of interlayer exchange interactions in magnetic multilayers, J. Phys. Condens. Matter. **11**, 9403 (1999).

[49] L. Fallarino, S. Stienen, R. A. Gallardo, J. A. Arregi, V. Uhlíř, K. Lenz, R. Hübner, A. Oelschlägel, O. Hellwig, and J. Lindner, Higher-order ferromagnetic resonances in out-of-plane saturated Co/Au magnetic multilayers, Phys. Rev. B **102**, 094434 (2020).

[50] L. Fallarino, B. J. Kirby, and E. E. Fullerton, Graded magnetic materials, J. Phys. D: Appl. Phys. **54**, 303002 (2021).
[51] P. Grünberg, R. Schreiber, Y. Pang, U. Walz, M. B. Brodsky, and H. Sowers, Layered magnetic structures: Evidence for antiferromagnetic coupling of Fe layers across Cr interlayers, J. Appl. Phys. **61**, 3750 (1987).
[52] P. Bruno and C. Chappert, Ruderman-Kittel theory of oscillatory interlayer exchange coupling, Phys. Rev. B **46**, 261 (1992).
[53] A. Fert, P. Grünberg, A. Barthélémy, F. Petroff, and W. Zinn, Layered magnetic structures: interlayer exchange coupling and giant magnetoresistance, J. Magn. Magn. Mater. **140-144**, 1 (1995).
[54] M. D. Stiles, Interlayer exchange coupling, J. Magn. Magn. Mater. **200**, 322 (1999).
[55] M. Rührig, R. Schäfer, A. Hubert, R. Mosler, J. A. Wolf, S. Demokritov, and P. Grünberg, Domain observations on Fe–Cr–Fe layered structures. Evidence for a biquadratic coupling effect, Phys. Stat. Sol. (a) **125**, 635 (1991).
[56] S. O. Demokritov, Biquadratic interlayer coupling in layered magnetic systems, J. Phys. D: Appl. Phys. **31**, 925 (1998).
[57] J. C. Slonczewski, Origin of biquadratic exchange in magnetic multilayers (invited), J. Appl. Phys. **73**, 5957 (1993).
[58] D. Bürgler, P. Grünberg, S. Demokritov, and M. Johnson, *Interlayer Exchange Coupling in Layered Magnetic Structures* (Elsevier, Amsterdam, 2001), Chap. 1, pp. 1–85.
[59] A. Kartsev, M. Augustin, R. F. L. Evans, K. S. Novoselov, and E. J. G. Santos, Biquadratic exchange interactions in two-dimensional magnets, npj Comput. Mater. **6**, 150 (2020).
[60] Y. Henry, O. Gladii, and M. Bailleul, Propagating spin-wave normal modes: A dynamic matrix approach using plane-wave demagnetizing tensors, arXiv:1611.06153.
[61] H. T. Nguyen and M. G. Cottam, The effect of lattice structure on dipole-exchange spin waves in ultrathin ferromagnetic films, J. Phys.: Condens. Matter **23**, 126004 (2011).
[62] X. M. Liu, H. T. Nguyen, J. Ding, M. G. Cottam, and A. O. Adeyeye, Interlayer coupling in $Ni_{80}Fe_{20}$/Ru/$Ni_{80}Fe_{20}$ multilayer films: Ferromagnetic resonance experiments and theory, Phys. Rev. B **90**, 064428 (2014).
[63] A. G. Gurevich and G. A. Melkov, *Magnetization Oscillations and Waves* (CRC Press, Boca Raton, FL, 1996).
[64] S. Klingler, V. Amin, S. Geprägs, K. Ganzhorn, H. Maier-Flaig, M. Althammer, H. Huebl, R. Gross, R. D. McMichael, M. D. Stiles, S. T. B. Goennenwein, and M. Weiler, Spin-torque excitation of perpendicular standing spin waves in coupled YIG/Co heterostructures, Phys. Rev. Lett. **120**, 127201 (2018).
[65] Y. Fan, J. Finley, J. Han, M. E. Holtz, P. Quarterman, P. Zhang, T. S. Safi, J. T. Hou, A. J. Grutter, and L. Liu, Resonant spin transmission mediated by magnons in a magnetic insulator multilayer structure, Adv. Mater. **33**, 2008555 (2021).
[66] H. Dötsch, P. Röschmann, and W. Schilz, Ferrimagnetic resonance spectra of magnetic bubble films at low microwave frequencies, Appl. Phys. **15**, 167 (1978).
[67] S. Sorokin, R. A. Gallardo, C. Fowley, K. Lenz, A. Titova, G. Y. P. Atcheson, G. Dennehy, K. Rode, J. Fassbender, J. Lindner, and A. M. Deac, Magnetization dynamics in synthetic antiferromagnets: Role of dynamical energy and mutual spin pumping, Phys. Rev. B **101**, 144410 (2020).
[68] O. Gladii, R. Salikhov, O. Hellwig, H. Schultheiss, J. Lindner, and R. A. Gallardo, Spin-wave nonreciprocity at the spin-flop transition region in synthetic antiferromagnets, Phys. Rev. B **107**, 104419 (2023).
[69] S. M. Rezende, C. Chesman, M. A. Lucena, M. C. de Moura, A. Azevedo, F. M. de Aguiar, and S. S. P. Parkin, Biquadratic coupling in sputtered Fe/Cr/Fe still in need of a new mechanism, J. Appl. Phys. **85**, 5892 (1999).
[70] P. Vavassori, M. Grimsditch, and E. E. Fullerton, Biquadratic exchange coupling in an unequal Fe/Cr/Fe(100) trilayer, J. Magn. Magn. Mater. **223**, 284 (2001).
[71] D. Mampallil, D. Aernout, and J. Meersschaut, Field-cooling effect in biquadratically interlayer-coupled Fe/Cr/Fe trilayers, Phys. Rev. B **75**, 060402(R) (2007).
[72] M. Li, J. Lu, and W. He, Symmetry breaking induced magnon-magnon coupling in synthetic antiferromagnets, Phys. Rev. B **103**, 064429 (2021).
[73] A. Sud, K. Yamamoto, K. Z. Suzuki, S. Mizukami, and H. Kurebayashi, Magnon-magnon coupling in synthetic ferrimagnets, Phys. Rev. B **108**, 104407 (2023).
[74] K. Yakushiji, A. Sugihara, A. Fukushima, H. Kubota, and S. Yuasa, Very strong antiferromagnetic interlayer exchange coupling with iridium spacer layer for perpendicular magnetic tunnel junctions, Appl. Phys. Lett. **110**, 092406 (2017).
[75] C. Dai and F. Ma, Strong magnon-magnon coupling in synthetic antiferromagnets, Appl. Phys. Lett. **118**, 112405 (2021).
[76] M. Belmeguenai, T. Martin, G. Woltersdorf, M. Maier, and G. Bayreuther, Frequency- and time-domain investigation of the dynamic properties of interlayer-exchange-coupled $Ni_{81}Fe_{19}$/Ru/$Ni_{81}Fe_{19}$ thin films, Phys. Rev. B **76**, 104414 (2007).
[77] T. Martin, M. Belmeguenai, M. Maier, K. Perzlmaier, and G. Bayreuther, Pulsed inductive measurement of ultrafast magnetization dynamics in interlayer exchange coupled NiFe/Ru/NiFe films, J. Appl. Phys. **101**, 09C101 (2007).
[78] M. Belmeguenai, T. Martin, G. Woltersdorf, G. Bayreuther, V. Baltz, A. K. Suszka, and B. J. Hickey, Microwave spectroscopy with vector network analyzer for interlayer exchange-coupled symmetrical and asymmetrical NiFe/Ru/NiFe, J. Phys.: Condens. Matter **20**, 345206 (2008).
[79] S. Bosu, Y. Sakuraba, K. Saito, H. Wang, S. Mitani, and K. Takanashi, Biquadratic exchange coupling in epitaxial Co_2MnSi/Cr/Fe trilayers, IEEE Trans. Magn. **44**, 2620 (2008).
[80] Y. F. Chiang, J. J. I. Wong, X. Tan, Y. Li, K. Pi, W. H. Wang, H. W. K. Tom, and R. K. Kawakami, Oxidation-induced biquadratic coupling in Co/Fe/MgO/Fe(001), Phys. Rev. B **79**, 184410 (2009).
[81] W. X. Xia, K. Inoue, S. Saito, and M. Takahashi, Effect of Rh spacer on synthetic-antiferromagnetic coupling in FeCoB/Rh/FeCoB films, J. Phys.: Conf. Ser. **266**, 012064 (2011).